Journal of King Saud University – Science 35 (2023) 102456

HOSTED BY

Contents lists available at ScienceDirect

Journal of King Saud University – Science

journal homepage: www.sciencedirect.com

Original article

Histopathological and hematological investigations of mice model inoculated with nickel oxide nanoparticles and bacterial pathogens: *In-vitro* and *in-vivo* antibacterial studies

Amreen Shah [a], Isfahan Tauseef [a], Muhammad Arfat Yameen [b], Manel Ben Ali [c], Sirajul Haq [d,*], Khaled Elmnasri [e], Mohammad S. AL-Harbi [c], Syed Kashif Haleem [a], Amor Hedfi [c], Mossadok Ben-Attia [f]

[a] Department of Microbiology, Hazara University Mansehra, 3100 Pakistan
[b] Department of Pharmacy, COMSATS University Islamabad, Abbottabad Campus, Islamabad, Pakistan
[c] Department of Biology, College of Sciences, Taif University, P.O. Box 11099, Taif 21944, Saudi Arabia
[d] Department of Chemistry, University of Azad Jammu and Kashmir Muzffarabad, 13100, Pakistan
[e] University of Manouba, ISBST, BVBGR-LR11ES31, Biotechpole Sidi Thabet, Ariana, Tunisia
[f] University of Carthage, Faculty of Sciences of Bizerte, LR01ES14 Laboratory of Environment Biomonitoring, 7021 Zarzouna, Tunisia

ARTICLE INFO

Article history:
Received 30 April 2021
Revised 1 October 2022
Accepted 15 November 2022
Available online 18 November 2022

Keywords:
Phytogenic synthesis
Nickel Oxide
Bacterial infection
Histopathology
Hematology

ABSTRACT

The *Paeonia emodi* (*P. emodi*) leaf extract was manipulated for the phytogenic fabrication of nickel oxide nanoparticles (NiO NPs) for *in-vivo* and *in-vitro* antibacterial activity against *Escherichia coli* (*E. coli:* (ATCC #: 15224)) and *Staphylococcus aureus* (*S. aureus* (ATCC #: 6538)). The surface area was found to be 78 m^2/g and was determined by the BET method using N_2 adsorption–desorption data. The cubic geometrical shape of NiO NPs was confirmed through X-ray diffractogram (XRD) analysis, and the enumerated crystallite size is 22.37 nm. The microstructure analysis was carried out via scanning electron microscopy (SEM), whereas the elemental composition was investigated by energy dispersive X-ray (EDX). The band gap energy of 1.93 eV was determined on the basis of the transmittance edge seen in the diffuse reflectance (DRS) spectrum. The surface functional moieties were identified by manipulating Fourier transform infrared (FTIR) spectroscopy. The MIC (minimum inhibitory concentration) value for *E. coli* (7.02 μg/mL) was found to be higher than that for *S. aureus* (3.51 μg/mL), whereas the dose-dependent *in-vitro* analysis was also carried out. In both bacteria, 3×10^7 CFUs was the tolerable concentration that causes maximum infection (no death) in mice. To explore the *in-vivo* therapeutic effectiveness of NiO NPs, 11 pm suspension was injected as the tolerated dose. The haematological and histopathological analysis discloses that the significant reduction in the bacterial infection was seen after the synchronous inoculation of NiO NPs and the bacterial suspensions.

1. Introduction

Multidrug resistant bacterial strains have been recognized as substantial nosocomial pathogens. The impotence to treat them with the traditional antibiotics is leading to a significant increase in the clinical impediment. There is an increased pervasiveness in the resistant strains because of exploitation of the antibacterial agents, so there is hasty requirement to come up with the antibacterial agents with an absolutely distinct mode of action and structure. Various mechanisms in the past few decades have failed to treat animals and humans because the extensive use of antimicrobials cause bacterial resistance as they are readily adapted to the changing environmental conditions (Arora et al., 2015). The exceptional development in the domain of nanotechnology could be manipulated to engender economical and novel antimicrobials. Metal and the metal oxide NPs have been extensively studied for the inhibition of bacterial growth as they are of small size and produce reactive oxygen species for bacterial inhibition (Ramalingam et al., 2019).

* Corresponding author.
E-mail address: cii_raj@yahoo.com (S. Haq).

Peer review under responsibility of King Saud University.

Production and hosting by Elsevier

https://doi.org/10.1016/j.jksus.2022.102456

At present metal oxide nanoparticles are considered to be entrancing materials because of their distinguishing applications in antibacterial, anti-fungal, electrochemical fields and the fields of food and sensors. They possess an extensive variety of applications regarding their enchanting chemical, electrical, optical and mechanical possessions. The shape, size, magnetic and electrical properties and large surface are the striking features that distinguish metal oxide nanoparticles from their bulk material. Among all other metal oxide NPs, NiO NPs have been engrossing on the account of their tunable and multifunctional nature (Maruthupandy et al., 2020). NiO is considered one of the most important transition metal oxide used for several applications and possess a cubic lattice structure. These NPs possess distinguishing chemical, thermal, physical, electrical, thermal and optical properties (Anand et al., 2020). Owing to their unmatchable flexible properties NiO NPs have fascinated the attention of most of the scientists and researchers these days. NiO has a wide band gap of 3.6 eV- 4.0 eV and is an intrinsic p-type semiconductor (Mayedwa et al., 2017). It has been abundantly manipulated for various applications in super capacitors, photocatalysis, lithium ion batteries, smart windows, catalysis of chemical processes, transparent conducting layers, solar thermal absorbers and electrochemical sensing. These NPs are also used in biomedicines owing to their anti-inflammatory property. They could also be utilized for the remediation of dyes and the environmental pollutants (Iqbal and Munir, 2019). Several methods like precipitation, hydrothermal synthesis, ball milling, sol–gel synthesis, gas deposition, electro-deposition and thermal decomposition method have been applied for the manufacture of NiO NPs, but most of them require sophisticated process and highly expensive instruments and are not environmental friendly. To get over the problem of toxicity and tedious instrumentation green method is highly preferred as it is non-toxic energy saving, cheap and also ecofriendly economic method (Anand et al., 2020; Lingaraju et al., 2020). Such environment benign method requires the manipulation of biological systems such as plants, fungi and the naturally available molecules like proteins and vitamins. Mainly, the plant extracts are prioritized as they act as the good capping and reducing agents (Ezhilarasi et al., 2020). Literature unveils that various plant materials are manipulated along with different precursor salts for the fabrication of NiO NPs. *Tamarix serotinaflower*, *Calotropic gigantean* with nickel nitrate as precursor salt, nickel chloride served as precursor salt with neem leaves and *Psidium guajava* and *Azadirachta indica* for the fabrication of NiO NPs. Similarly, *Callistemon viminalis* and Arabic gum have been used with nickel nitrate and nickel chloride respectively, for synthesizing metal oxide NPs (Isa khan et al., 2020).

In the current investigation, the extract from *P. emodi* leaves was used as a reducing and capping agent in the environmentally friendly production of NiO NPs. The Paeoniaceae plant *P. emodi* is typically found in the mountainous areas of northern Pakistan and is used there to treat colic, hypertension, and asthama. Utilizing techniques such as N2 adsorption–desorption, SEM, XRD, DRS, EDX, and FTIR, the physiochemical characteristics of the NiO NPs were examined. The 96 well plate and the well diffusion techniques were used in the MIC and in-vitro experiments respectively. Mouse models were injected with various quantities of the selected bacteria and NiO NPs to determine in-vivo tolerance. The symbiotic relationship between bacteria and NiO NPs was evident from the histopathological and haematological investigations.

2. Materials and methods

2.1. Reagents used

The analytical quality reagent were provided by Sigma-Aldrich, including ethanol, nickel nitrate hexahydrates, iodonitrotetrazolium chloride, and agar nutrients. While all of the required solutions were prepared in double distilled water, the NiO NP suspensions for in-vivo and in-vitro testing were made with regular saline. After washing with a fifteen percent (v:v) HNO_3 solution, the glassware was thoroughly rinsed using double distilled water. The chosen bacteria species were supplied by the department of pharmacy.

2.2. Extract preparation

To remove dust particles, the healthy *P. emodi* leaves were thoroughly cleaned three times: once with regular water, twice with deionized water. To preserve all the chemical components including chlorophyll, the leaves were shade-dried. Using a sterile grinder, the leaves were reduced to small bits, and 10 g of the reduced leaves were added to a titration flask that held 200 mL of boiling deionized water. Aluminum foil was used to tightly seal the titration flask for a period of 12 h. The top transparent layer of the greenish crude extract was removed, centrifuged for 15 min at 4000 rpm, and then stored at 4 °C.

2.3. Synthesis of NiO NPs

In 500 mL of deionized water, 0.73 g of nickel nitrate hexahydrate was dissolved to create a 5 mM stock solution. For the creation of NiO NPs, 45 mL of the stock solution and 15 mL of *P. emodi* leaf extract were homogenized under stirring. A suitable quantity of NaOH solution was added to keep the pH at 10. At 50 °C, the reaction mixture was stirred for 90 min and was then allowed to cool at room temperature for 24 h. Centrifugation was used to separate the solid product, which was extensively cleaned with deionized water before being treated with analytical grade ethanol. In an electric oven, the resultant product was dried at 100 °C before being stored in a sealed sample vial.

2.4. Characterization

The N2 adsorption–desorption examination was done using the GeminiVII2390i instrument, and the data acquired was processed by utilising BJH and BET techniques to determine the textural parameters, viz., pore size and surface area. The crystallographic parameters were determined by manipulating the Panalytical X-pert Pro in the 2-theta range 20°–80°, and the crystallite size was enumerated using the full width and half maximum (FHWM) values. The surface morphology was investigated using the Japanese-made SEM model 5910 and the TEM (HRTEM, JEM-2010). While the surface chemical moieties were classified using FTIR analysis (Nicolet 6700 (USA)), the elemental composition was ascertained using EDX and SEM (model: INCA 200 (UK)).

2.5. MIC assay

A 96-well plate technique, commonly known as an ELISA, was manipulated to conduct the MIC (minimum inhibitory concentration) experiment, and 100 µL of the broth medium was applied to 72 wells in columns 1 to 9. The antibiotic solution (256 µg/mL) was put into 24 wells (columns 10 to 12) in triplicate, while 100 µL of NiO NPs (1024 µg/mL) were placed in 48 wells (columns 1 to 6) and each row contain 100 µL. The 100 µL bacterial suspension and the microbial suspension of *S. aureus* and *E. coli* in normal saline were collated. The first three columns were filled with the *S. aureus* suspension, and the following column was filled with the *E. coli* suspension. The columns containing bacterial suspension, which serve as an indication of the non-inhibitory concentration of NiO suspension, were combined with the 40 µL iodonitroterazolium chloride (INT) solution (1 mg/5mL). Prior to the row where

the colour changed, the lowest concentration row is where the MIC value was recorded.

2.6. In-vitro antibacterial study

The synthesizrd NiO NPs was screened against the selected bacteria following agar well diffusion procedure and the Agar nutrient was employed as a substrate for antibacterial susceptibility testing. Clinical strain was generated using the 0.5 McFarland solution, and the NiO suspensions were made by dispersing one, two, three and four milligrams in one milliliter of normal saline. With the use of sterile swabs, bacterial pathogens were streaked over the medium and sterile borer was used the dig the well having 8 mm diameter. Every well was then separately filled with 100 L of each suspension before being incubated at 37 °C. After 24 h, the activity of NiO NPs against certain bacteria was evaluated using the zone of inhibition, which is quantified in millimetres (mm).

2.7. Tolerance study

According to the local ethics commission, all animal experiments were carried out. In this investigation, female mice weighing 20–22 g and aged 6–8 weeks were employed. The mice were assigned at random to five groups of five, with n = 5 in each group. Different quantity of the prepared NiO Suspensions (1, 2, 3, 4 and 5 ppm) and microorganism broth (1×10^7, 2×10^7, 3×10^7, 4×10^7, and 5×10^7 CFUs/mL) were administered to model organisms (n = 5). The behaviours of the model organisms were observed for the first four hours and then For future research, the highest dose of nanoparticles and bacterial solution that allows mice to live for 14 days was used.

2.8. In-vivo antibacterial study

For *in-vivo* antibacterial tests, wholesome, pathogen-free mice that were at the age of 6–8 weeks and weighed about 20–22 g were used. Mice models were concurrently given a specified amount of NiO NPs (11 ppm) and bacterial solutions (3 × 107 CFUs). The effectiveness of NiO NPs was evaluated by contrasting the histopathological and haematological results of infected mice with those that had simultaneously been injected with bacteria and NiO NPs.

2.9. Histopathological study

For histopathological study, the selected organs were the lung, spleen, liver, and kidney. A trifling part of these organs was served with 10 % formalin and later with paraffin, followed by cutting them down to 5–6 mm (mm) sections using the standard histopathological process, and then fastened on the glass microscopic slide (Mushtaq et al., 2017). The slices were stained with hematoxylineosin and seen under a light microscope.

2.10. Hematological study

After anticoagulation, the blood was sampled from the hearts of mice that had been given injections of specified amounts of NiO NPs and bacterium suspensions, as well as animals that had been infected with various bacterial species. Blood parameters including haemoglobin (HGB), platelet count (PLT), mean platelet volume (MPV), average corpuscular haemoglobin concentration (MCHC), Mean corpuscular haemoglobin (MCH), mononuclear percentage (MOD%), granulocyte percentage (GRN%), average corpuscular volume (MCV), and lymphocyte percentage (LYM%) were studied using the automatic haematology analyzer (MEK-6318 K).

3. Results and discussion

3.1. Physico-chemical study

The type IV (a) N_2 adsorption/desorption isotherm shown in Fig. 1, exhibits a rounded lower knee, suggesting that the mesoporous nature of NiO NPs. The isotherm exhibits maximum adsorption ranging from 0.5 to 0.8p/p°, leading to the formation of an H2 (b) hysteresis loop, which is associated with pore blockage. The BET surface area calculated was 78 m^2/g with pore size and pore volume of 18.12 nm and 0.327 cc/g, respectively.

The XRD pattern of NiO NPs reveals three diffraction peaks with corresponding hkl values of (111), (200), and (220) at 37.32, 43.36, and 62.94 as shown in Fig. 2a. The cubic geometry of the synthesized NiO NPs was confirmed by the peaks and hkl values, which corresponded with peaks noted on JCPDS card 01–073-1519. The crystallite size of 22.37 nm and the crystallographic defect of 0.401 % were determined by the Debye-Scherrer equation. The presence of elements in the sample, their percentage and purity of NiO NPs was explored by using an EDX analysis (Fig. 2b). The intense Ni peaks at 0.8, 7.9, and 8.5 keV, as well as a signal at 0.6 keV ascribed to O and a band at 0.4 keV assigned to C, are visible in the EDX spectrum of the examined sample. Ni, O, and C all have weight percentages of 73.4, 25.2, and 1.4 %, respectively. The carbon tape used to stack the samples caused the C peak in the spectrum (Anand et al., 2020).

The morphology of NiO NPs was extracted from the low and high-magnified SEM micrographs given in Fig. 3(a and b). The low magnification SEM micrograph (Fig. 3a) shows mixed morphology of the sample. Many small sized particles are irregularly scattered led to the formation of porous like structure while other are closely connected with one another, forming larger sheet like structures. The high magnified SEM (Fig. 3b) shows that the particles with visible boundaries are closely connected with each other, although some cavity are also seen due to the uneven distribution of the NPs. The non-uniform size and shape of the particles are due to the interaction of the NPs to each other through weak attractive forces (Hafeez et al., 2021). An SEM micrograph revealed NPs sizes ranging from 21.74 to 89.57 nm, with an average size of 58.86 nm (Fig. 3b). The wide size range of several NPs are due to the dehydration of the sample and it also believed that the NPs has high

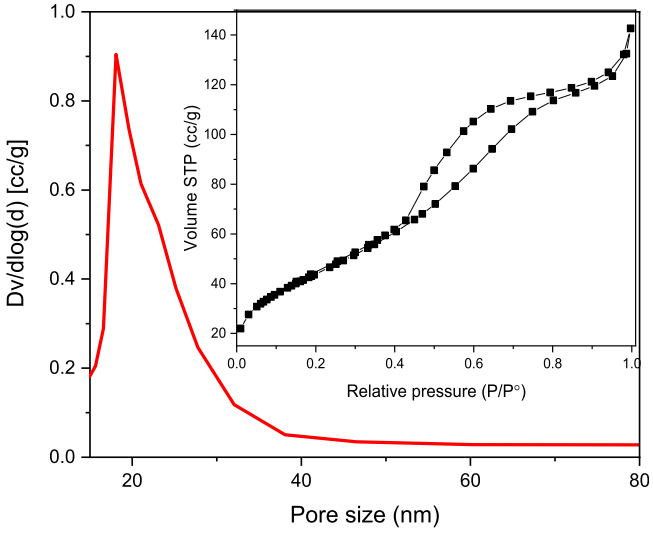

Fig. 1. Pore size distribution (inset: N2 adsorption–desorption isotherm) curve of NiO NPs.

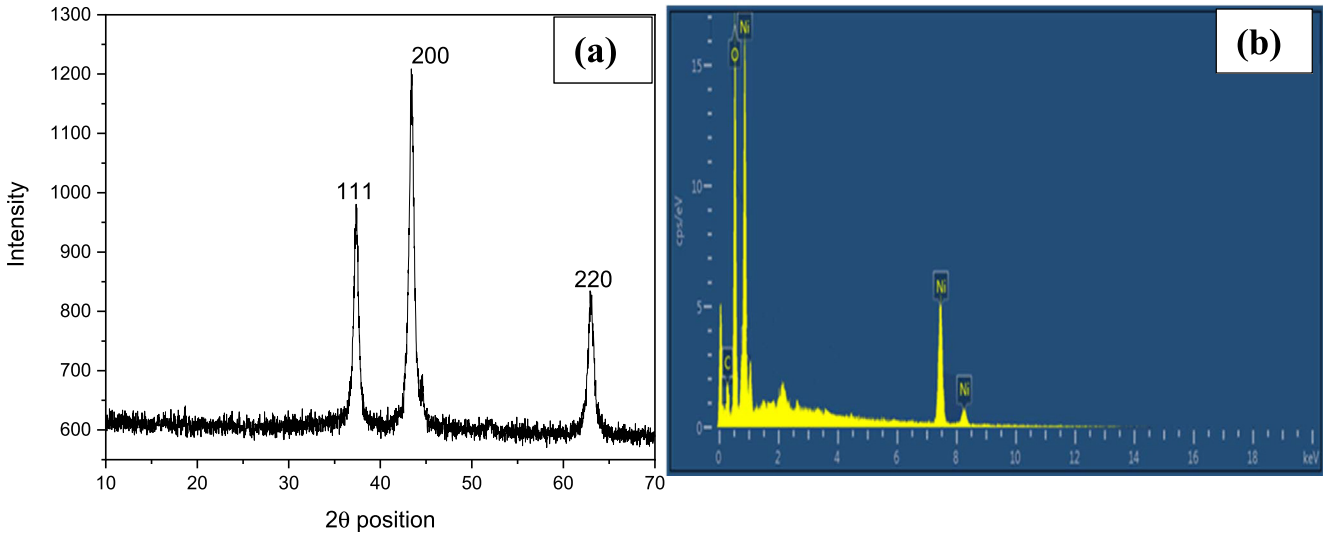

Fig. 2. XRD diffractogram (a) and EDX spectrum (b) of NiO NPs.

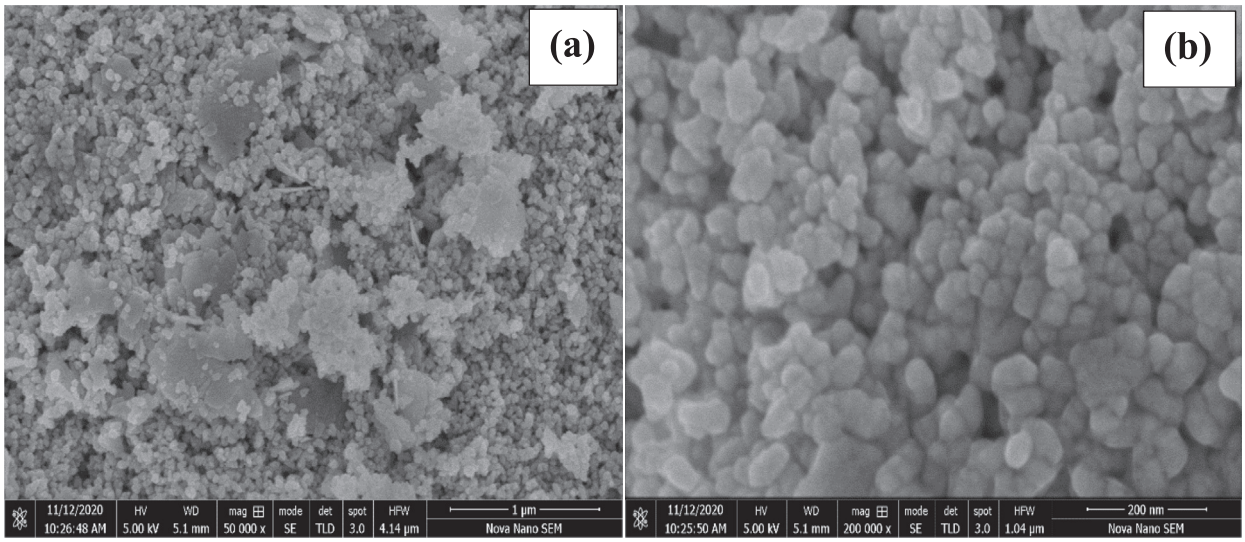

Fig. 3. Low (a) and high (b) SEM micrographs of NiO NPs.

surface energy and by aggregates formation the NPs disintegrate their energy and become stable (Saravanan et al., 2018).

The DRS spectrum of NiO NPs exhibited in Fig. 4 (a) illustrates that the highest absorption turned out to be in the visible range, which is responsible for the excitation of election to conduction band from valance band. The wavelength of the transmittance edge for NiO NPs is 645.01 nm and was calculated by joining the sharp rising portion with X-axis of the UV–vis plot according to the previous finding. (Haq et al., 2018). The band gap of NiO NPs was found to be 1.47 eV as its evident from the Tauc's plot (inset: 4), which is less than that reported in literature (Haq et al., 2021b). In the FTIR spectrum of the NiO NPs exhibited in Fig. 4 (b), a low intense at 3702.05 cm^{-1} is due to non-bonding water molecules. The broad absorbance band centered at 3455.99 cm^{-1} is accredited to the vibration of O—H moiety, whereas the peak at 1636.39 cm^{-1} is assigned to the bending vibration of water molecule (Haq et al., 2021a). The peak at 1395.03 cm^{-1} was attributed to the NO_3 moiety, which could be due to the use of nickel nitrate salt (Rehman et al., 2021), whereas the band at 1242.57 cm-1 is ascribed to the vibration of the terminal $Ni(OH)_2$ (Angel Ezhilarasi et al., 2018). The band at 1096.85 cm^{-1} and 1031.19 cm^{-1} is assigned to the strong extending vibration of Ni-O, whereas the bands at 548.56 cm^{-1} and 439.39 cm^{-1} are the wagging and bending vibrations of Ni-O (Haq et al., 2021b).

3.2. MIC results

The important aspect of antibacterial activity is to determine the minimum amount of the antibacterial agent that restricts the growth of treated bacterial species. The MIC experiment was executed to estimate the minimum quantity of NiO NPs that controls the growth of both *E. coli* and *S. aureus*. During the current experimental condition, the coloured wells show that the amount of NiO NPs is enough to stop the growth of bacterial pathogens, whereas the colour wells indicate the quantity of NiO NPs is too small to control bacterial growth. The amount in the wells just before the coloured well is considered the MIC of NiO NPs against each bacteria. The results show that 3.51 µg/mL and 7.02 µg/mL are the minimum quantities of NiO NPs that totally restrict the growth of

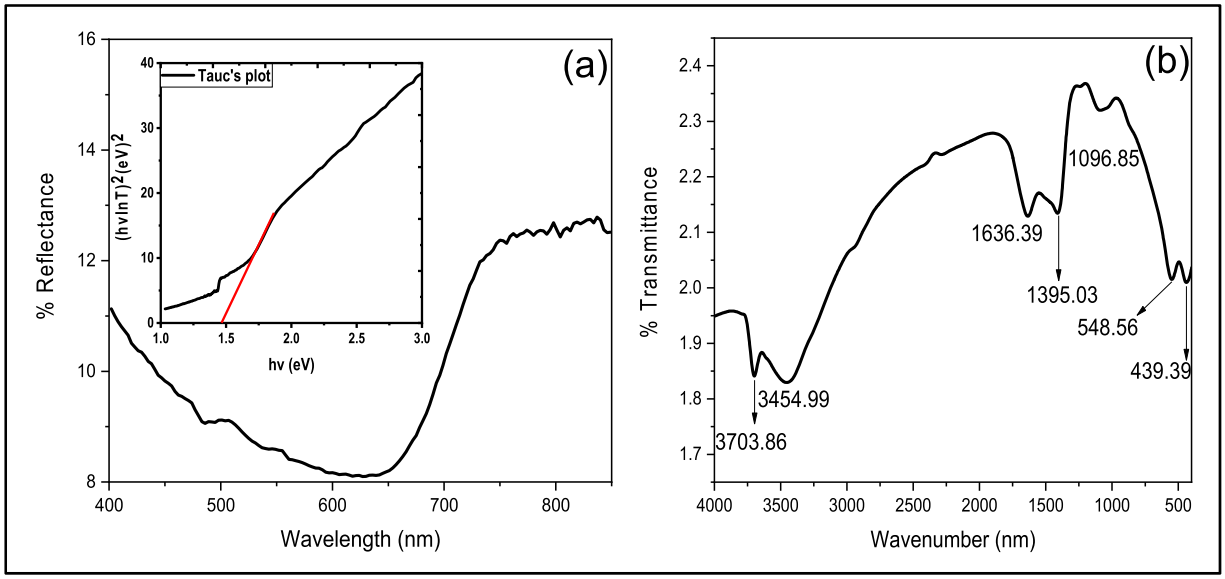

Fig. 4. DRS (*inset:* Tauc' plot) (a) and FTIR (b) spectra of NiO NPs.

E. coli and *S. aureus* under the current experimental context, respectively.

3.3. In-vitro antibacterial activity

The antibacterial screening of NiO NPs was carried out against Gram negative bacteria (GNP) and Gram positive bacteria (GPB) and the obtained experimental photographs of concentration-dependent antibacterial activity are given in Fig. 5 (a and b) shows high activity against both bacteria at higher concentration. This rise in activity can be attributed to the abundant quantity of NiO NPs available in the suspension that can encounter the bacterial growth. Based on the measured inhibition zones, the activity of NiO NPs was found greater against GPB than GNB comparatively. Similar results were also obtained during the MIC experiment, where 3.51 µg/mL and 7.02 µg/mL are the inconsiderable amounts of NiO NPs that restrict the growth of *S. aureus* and *E. coli,* respectively. This contrast in the activities may be attributed to the dissimilarity in the cell wall composition of GNB and GPB of both bacteria. Cell wall of the GPB is solid, consisting of manifold layers of teichoic acid, peptidoglycan, and lipoteichoic acid. Lipoteichoic acid and teichoic acid serve as the chelating agents which capture the Ni cation from NiO and penetrate it within the cell. The cell wall of GNP consists of several peptidoglycan layers with an outer membrane. The major constituents of the outer membrane are lipoproteins and the lipopolysaccharides, and the peptidoglycan interact with lipoproteins in fluids including periplasm and allowing the transport of NiO (Haq et al., 2021a). GPB bears a partial + ve charge due to the presence of phosphate ions, while lipopolysaccharide and phospholipids provide GNB with a heavy negative surface charge. Resultantly, the electrostatic interaction of the Ni^{2+} ions in the suspension promptly interferes with –ve charged bacterial surface, and as a result the biochemical nature of disturbed. The GNB cell wall is relatively thinner than the GPB cell wall comparatively, so the capacity of penetration of Ni^{2+} into the inside of GNB is higher than GPB. In this process, the O2 is also released and by reacting with water produces the hydrogen peroxide that kills the pathogens after penetrating them (Shah et al., 2019; Zarei et al., 2020).

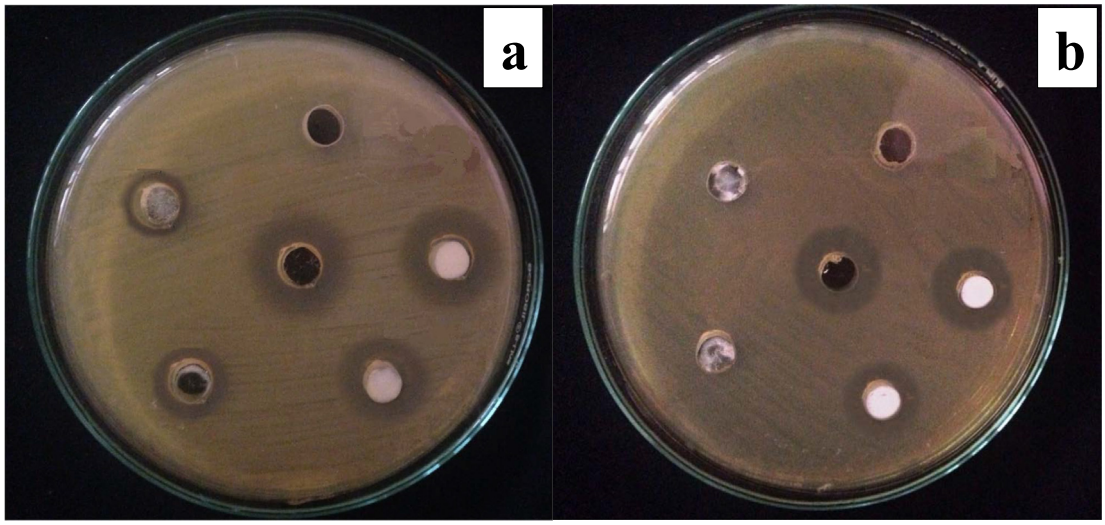

Fig. 5. Pictorial representation of antimicrobial activity of NiO NPs against selected bacteria; a = *S. aureus; b = E. coli.*

3.4. Tolerance study

3.4.1. Histopathological analysis

The tolerance of the mouse model to NiO NPs was study by inoculation of five, ten, fifteen, twenty and twenty-five ppm suspension into five mice groups (where each group has five members), and behavior observation for fourteen days. Mice exposed to 10 ppm survive for 14 days, whereas those exposed to 20 and 25 ppm either pass away right away or over the course of many days. Severe skin infections, thirst, and a progressive weight loss were all observed in mice fed with a 15 ppm solution, which may have been caused by the mice's diminished appetite. The group's other two members survived for a total of 14 days with very minimal odd behaviour, while two of them passed away after just 10 days and the third after 13 days. It is clear from this that the concentrations beyond 15 ppm did not have an impact on the current experimental design. The precise acceptable dose of NiO NPs was next examined by injecting 11, 12, 13, and 14 ppm into four groups of mice. In contrast to those infected with 12 ppm, which showed severe skin infection, dehydration, and weight loss, and two mice in the group died on the 13th day, the groups receiving injections of 13 and 14 ppm all perished on the 14th day. The mice given an 11 ppm vaccination showed signs of skin infection, weight loss, and sleepiness, but they survived for fourteen days. To determine the effect of the NiO NPs on the various organs of mice model, histopathological analysis was done on the control, tolerated group (11 ppm; whereas the infected mice reverted to normal condition after few days), and maximum dosed group (14 ppm; fatal dose resulted in death) groups. The results of the mice models dosed with NiO NP suspensions at 11 and 14 ppm are shown in Fig. 6, along with a comparison of histological findings in the liver, kidney, spleen, and lung.

In the kidney section shown in Fig. 7, no major difference was found beside a mild congestion among the control group and the one exposed to tolerated dose. A degenerative alteration with frequent leukocytic infiltrations was observed in the tubular epithelial cells. The metabolic irregularity in the mice was because of necrosis in the tubular epithelium (Ahmadmoradi et al., 2012; Gad and Zaghloul, 2013; Jasper et al., 2012). Following inoculation with an 11 ppm NiO suspension, a little bleed was noticed in the parenchyma of the spleen. In contrast to damaged blood vessels in the spleen segment, significant leukocyte infiltration was visible in the splenic parenchyma of mice infected with a fatal dosage. Mice given an 11 ppm solution of NiO NPs had bronchioles that were almost perfectly normal in morphology and just slightly infiltrated with leukocytic cells in the lung region. Mice implanted with a fatal dosage of NiO NPs had significant leukocytic infiltration in the lung region due to coagulation in the epithelial linings of the bronchi and total bronchial destruction (Gad and Zaghloul, 2013; Wang et al., 2017). The gross lesions are swollen and a damaged lung with ruptured fibrin was seen, which merged together to form a bullae (Gao et al., 2013). The dreadful inflammation of the alveolar septa lead to the pathological abrasion resultantly followed by a total damage (Chen et al., 2007). Besides the minor lesion and hemorrhages, the hepatocytes are visualized to be normal after inoculation of a tolerated dose. The extensive lesions with moderate hemorrhage was visualized in liver after giving a dose of 14 ppm suspension of NiO NPs. Several focal hemorrhagic and necrotic areas were seen in the liver, where necrotic foci and polymorph nucleated cells are scattered (Gad and Zaghloul, 2013; Llobet et al., 1988). Due to bursting blood vessels, extreme petechiae and purpura hemorrhage was noticed in the kidney, spleen, liver and lungs sections of mice loaded with lethal dose.

Inoculation of various bacterial suspensions, namely 1×10^7, 2×10^7, 3×10^7, 4×10^7 and 5×10^7 CFUs, was used to examine the immunity of mice against the selected bacteria. Five group of mice (n = 5) were given separate *S. aureus* suspensions and their behavior were noticed for 14 days. Under a light microscope, the

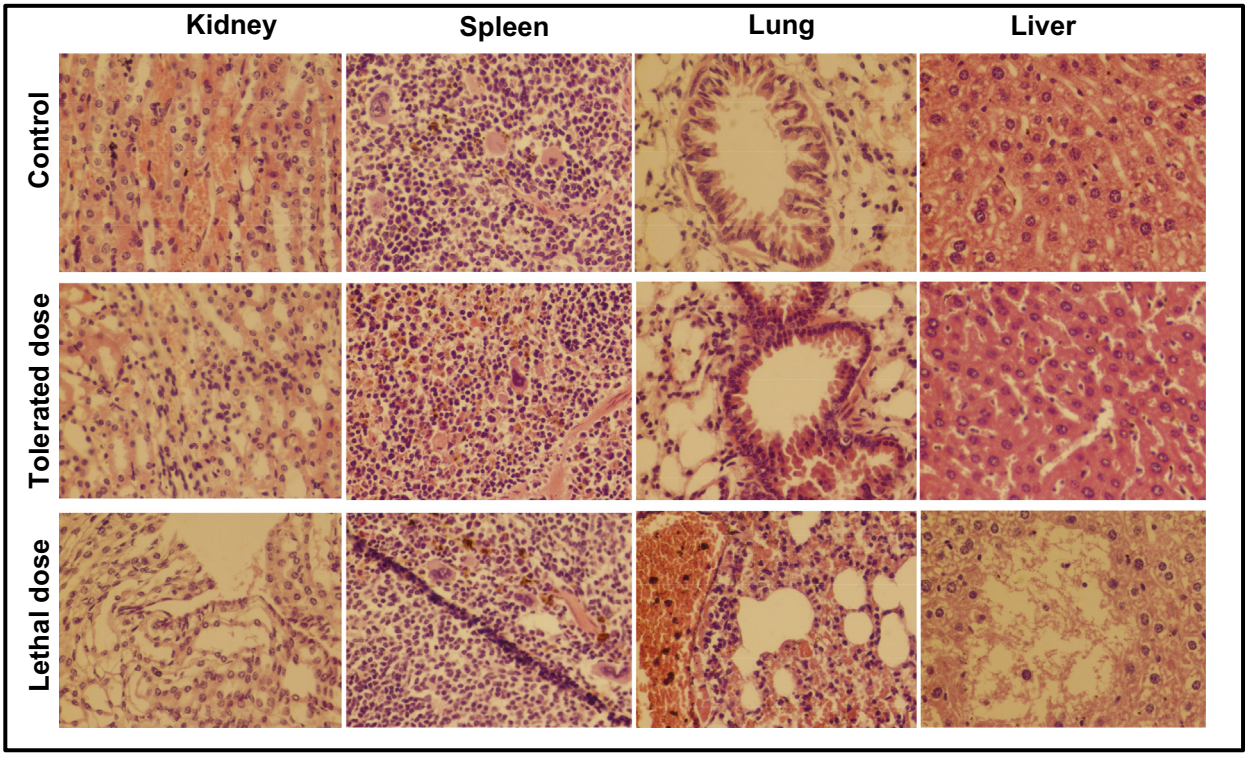

Fig. 6. Histopathological examination of kidney, spleen, lung and liver of mice injected with low and high dose of NiO NPs for 14 days; tolerated dose (11 ppm) and lethal dose (14 ppm).

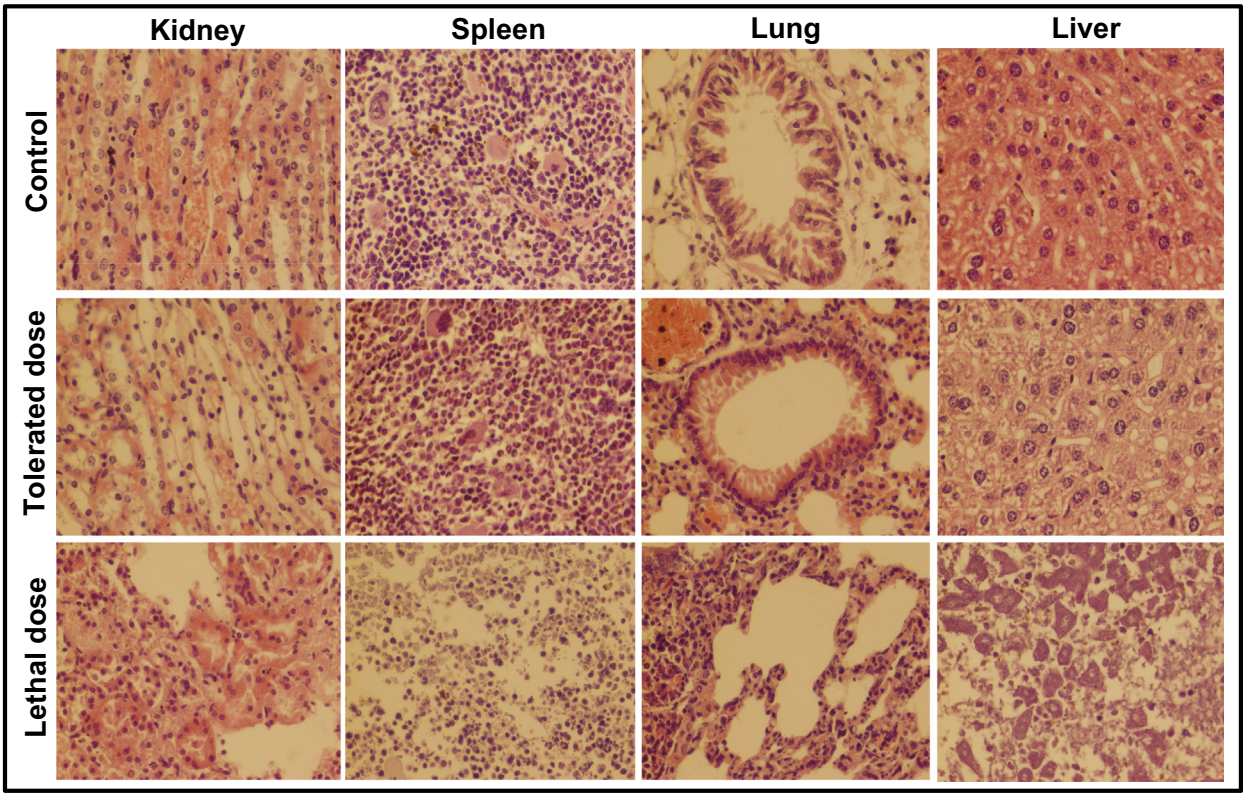

Fig. 7. Histopathological examination of kidney, spleen, lung and liver of mice injected with low and high dose of *S. aureus* inoculums for 14 days; (Tolerated dose = 3 × 107 CFUs; Lethal dose = 4 × 107 CFUs).

kidney, liver, spleen, and lung of mouse models injected with tolerated dose with tolerated dose (3×10^7 CFUs) and lethal dose (4×10^7 CFUs) were tested, and the results are exhibited in Fig. 7. The inoculation of *E coli* suspension was done in the same way, and the findings are seen in Fig. 8. The mice loaded with the lethal dose had noticeable signs such as ineffective action, skin inflammation, and weight loss, which faded with time. The symptoms observed in the mice unveiled to the tolerated dosage are low food consumption, dehydration, gradual weight loss, and uncontrolled breathing, however these mice survived for fourteen days.

Mice inoculated with the tolerated doses of both bacterial suspensions exhibited moderate necrosis and congestion on the parenchymal surface, while mice exposed to a lethal dose showed glomerular degeneration, severe necrosis, and high degrees of infiltrations. The spleen of mice inoculated with 3×10^7 CFUs of S. aureus was seen normal where a medium degree hemorrhage was observed in the spleen of mice injected with 3×10^7 CFUs of *E. coli.* A severe leukocytic infiltration in the parenchyma and hemorrhage was examined on the capsular spleen surface upon the inoculation of 4×10^7 CFUs of both bacteria. At low doses, lung cells showed a slight broadening of the alveolar septum and lymphocyte intrusion, while at high doses, substantial dilation and massive lymphocyte impaling result in ultimate destruction of lung cell (Hunter et al., 1973). An extreme petechial and puerperal hemorrhage was observed in kidney, spleen and liver section, which might be due to bursting blood vessels. In contrast to the control group, the moderate infection was found in the tissue of the scrutinized mice organs treated with a tolerated dose. Histopathological examination revealed the extremely abnormal condition of mice organs exposed to high concentrations of NiO NPs and bacterial suspensions.

The *in-vivo* therapeutic study of NiO NPs against the selected pathogens was carried out by synchronous injection of 11 ppm of NiO and 3×10^7 CFUs of bacterial suspension and the liver, spleen, lungs and kidney of mouse models was histopathologically examined as demonstrated in Fig. 9. After the synchronous vaccination of NiO NPs and bacterial suspension, the mice seemed disturbed and were not attracted to food for a few days. The abnormal behavior along the moderate skin infection was seen in the in the mice simultaneous inoculated with both bacteria and NiO suspensions. However, the mice injected with *E. coli* and NiO suspension had abnormal breathing, drowsiness, and nervousness for a longer time period than those injected with S. aureus and NiO suspension. Both of these symptoms persisted for fourteen days, but their severity decreased with time, whereas the speedy recovery was noticed in the mice unveiled to *S. aureus* and NiO suspension. The liver, spleen and lung of mice injected with *S. aureus* and NiO suspension showed mild improvements, while the kidney portion showed no infection. After the simultaneous inoculation of bacterial and NiO suspensions, the ratio of petechial and puerperal hemorrhage in tissue parts decreased. The irregular breathing of both mouse models may be due to a mild infection found in the lung section, where a moderately distressed respiratory bronchiole with the alveoli was found in the lungs of mice injected with *S. aureus* and NiO NPs. The livers of both mouse models showed minor congestion and haemorrhage with no morphological symptoms. However, the haemorrhage was more severe in the mice uncovered to *E. coli* and NiO NPs. A moderate kidney obstruction along with a minor liver hemorrhage was also noticed in mice doses with *E. coli* and NiO NPs. These findings show that the extreme infections/-damage found during the tolerance analysis after the inoculation of bacterial pathogens is reduced after the simultaneous injection

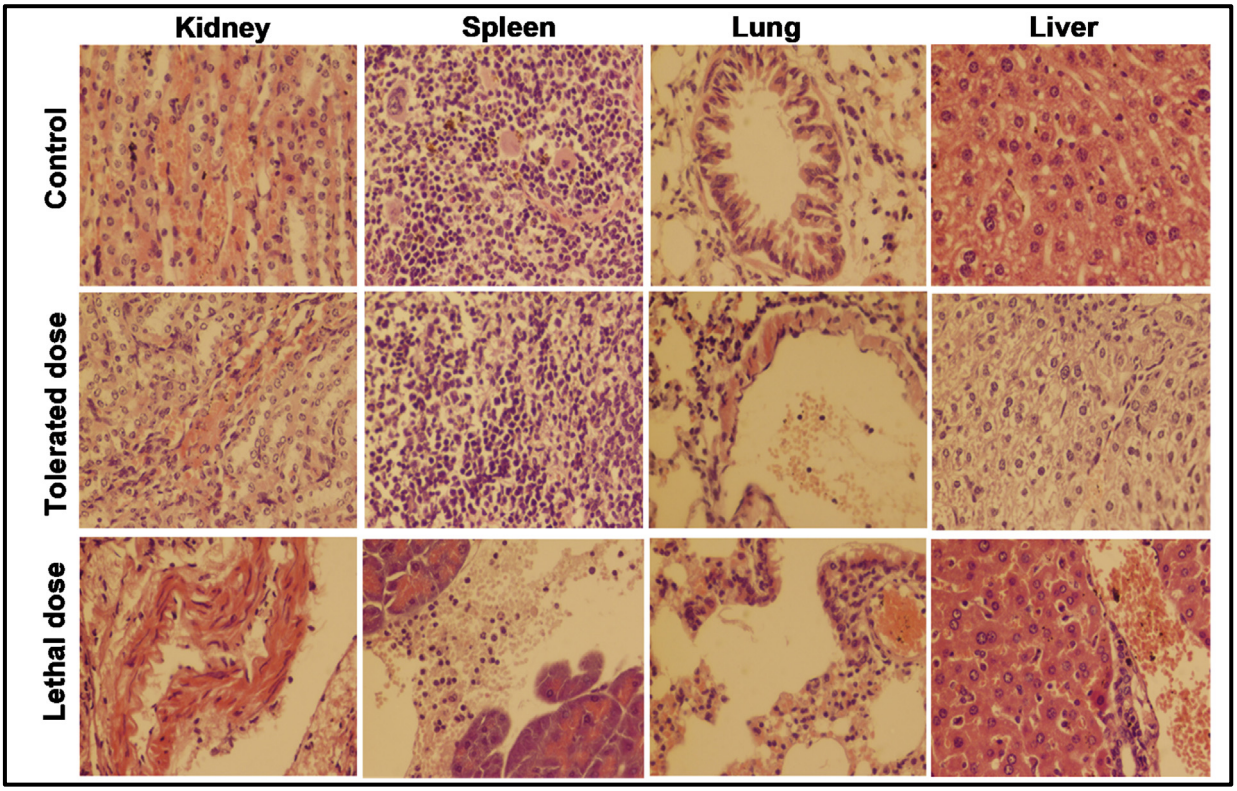

Fig. 8. Histopathological examination of kidney, spleen, lung and liver of mice injected with low and high dose of *E. coli* inoculums for 14 days; (Tolerated dose = 3 × 107 CFUs; Lethal dose = 4 × 107 CFUs).

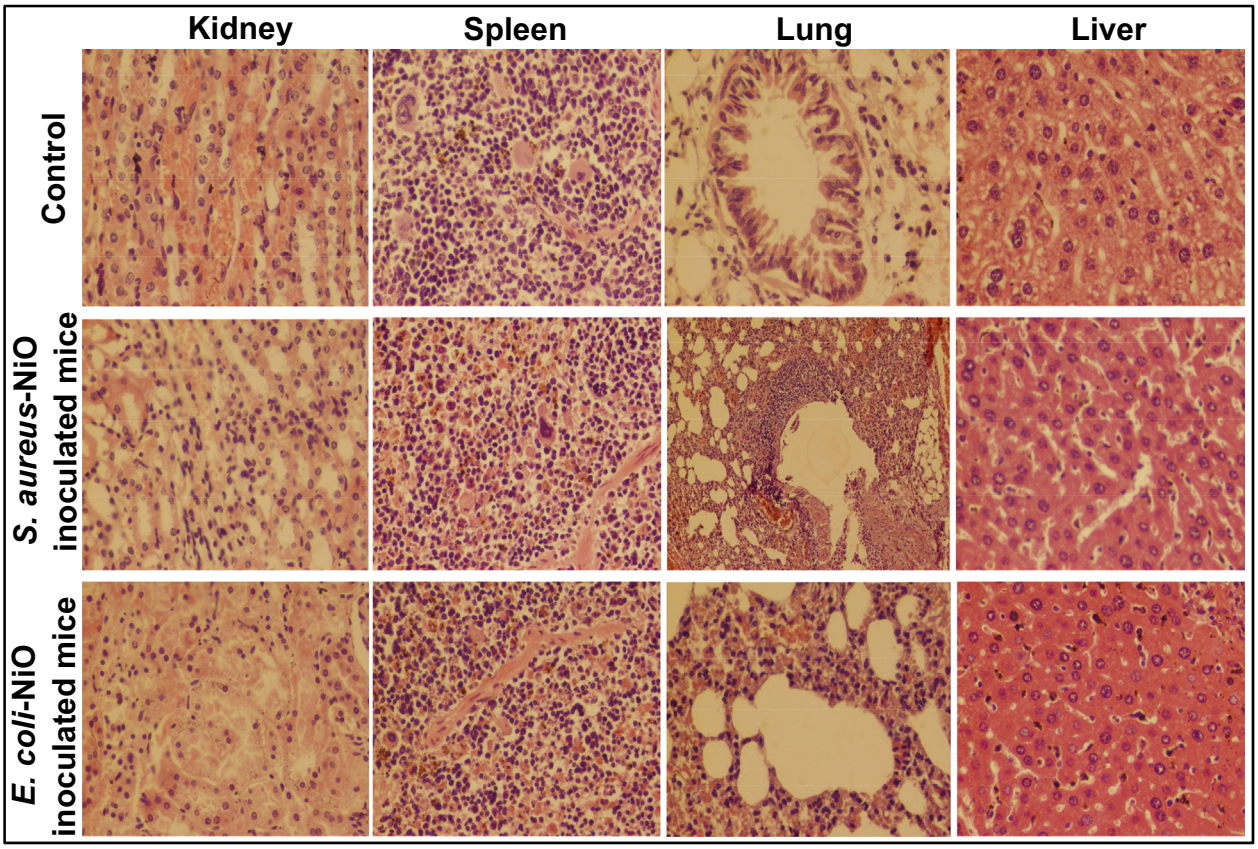

Fig. 9. Histopathological examination of kidney, spleen, lung and liver of mice simultaneous inoculated with tolerated concentration of both NiO NPs (1 ppm) and bacterial suspension 3 × 10^{-7} CFUs).

of NiO NPs and bacterial suspension. All of the findings point to the inoculation of NiO NPs having a minor therapeutic effect against such pathogens.

3.4.2. Hematological analysis

Infected mice and mice that were simultaneously injected with bacteria and NiO NPs underwent a haematological study. Blood samples from mouse hearts are measured after anticoagulation. An automated hematology analyzer was used to determine blood parameters viz., RBC, WBC, MCV, MCHC, MCH, PLT, MPV, HGB, RDW, LYM percent, GRN percent, and MON percent (MEK-6318 K). The blood hematological analysis of mice exposed to NiO NPs and pathogenic suspension shows some important improvements. Some blood parameters of infected mice, such as WBC, lymph, GRAN#, MON#, GRAN%, MON%, PLT, and RDW were significantly higher than normal values, while MCV, MCH, and MCHC were significantly lower than normal values, as seen in Table 1.. The NPs are thought to have entered the lungs and were passed into the blood circulation system by splitting the alveolar cell, disrupting the hematological system (Al-Qayim et al., 2014).

Leukocytosis, or a high WBC count, is a sign of both bodily and mental distress and shows that the immune system is battling an infection. Additionally, it has been discovered that a particular blood cancer-related bacterium may have a high WBS count. Idiopathic hypereosinophilic syndrome can cause edoema, weight loss, rash, unconsciousness, confusion, and weakness by damaging the nervous system, skin, lungs, liver, and heart (Shanker et al., 2017). Monocytosis is a usual symptom of chronic myelomonocytic leukemia, a form of leukaemia in which the blood is produced in the bone marrow. Meanwhile, new research suggests that an increased monocyte count is linked to some cardiovascular diseases (Gad and Zaghloul, 2013; JENG and SWANSON, 2006). Granulocytes are white blood cells (WBCs) with small granules that help the body combat viral and bacterial infections. The increase in the number of granulocytes (granulocytosis) for infections, blood cell cancers, and autoimmune diseases, causes the organism to experience excessive sweating during sleep, abnormal breeding, loss of appetite, fatigue, and pale skin (Akah and Alemji, 2009).

Red blood distribution width (RDW) blood testing determines the amount of red blood cells (RBCs), which is estimated and is over the normal range due to nutritional deficiencies (vitamin B-12, iron, and foliate deficiency), parasite, liver and cardiac problems, cancer, and anaemia (Wang et al., 2017). A low RDW would be expected given the high RDW and low MCV, which point to microcytic anaemia brought on by RBC shortage (Chen et al., 2007). When liver cells are damaged, a substance called alanine aminotransferase (ALT) is released into the bloodstream, which can cause symptoms such as jaundice, lack of appetite, fatigue, stomach discomfort, vomiting, and nausea in the organism. A high ALT level is a sign of liver distress brought on by cirrhosis, hepatitis, liver cancer, or using medications that cause liver infections (Rodrigues et al., 1995). The ratio of RBCs in the body is measured by the hematocrit test (HCT), and high readings point to polycythemia, dehydration, and lung and heart diseases. The type of anaemia that an organism has can be determined by looking at the mean MCV, or average RBC size, and the range of MCV. Microcytic anaemia is a form of anaemia in which the RBCs are too small because of lead poisoning, iron deficiency(low iron consumption in the diet, gastrointestinal/menstural bleeding), thalassemia, or other chronic disease (Kelly Nitsche, 2004). The overall amount of haemoglobin in the body's RBCs is represented by the mean MCH. The major causes of low MCH are celiac disease, iron deficiency, microcytic anemia and symptoms such as gasping, lack of normal stamina, regular tiredness, dizziness, body fatigue, and skin infection can occur when the level of MCH is lacking (Teeguarden et al., 2007). The mean MCHC is the average amount of haemoglobin present in a single RBC. Fatigue, gasping, light skin, dizziness, easily bruised, and exhaustion are all symptoms of a low MCHC level. Hypochromic microcytic anemia, which is caused by a hemolysis, peptic ulcer and lack of iron is the most frequent cause of low MCHC. Rapid breathing, a high heart rate, confusion, coughing, sweating, wheezing, and gasping are all symptoms of this form of anemia (Hein, 2003). All of these findings indicate that the infection in mice was exacerbated by the introduction of bacterial pathogens. The *in-vivo* therapeutic action of NiO NPs against bacterial infections was performed, together with data obtained from haematological analysis of blood samples from severely sick mice that weren't killed after receiving NiO NP treatment. The WBC, Lymph, MON#, MON%, and MCV increased/decreased estimates were observed to be practically within the standard range, demonstrating the therapeutic value of NiO NPs. After the synchronous inoculation of NiO NPs and bacterial pathogen, the deviated values of RDW, MCHC and GRAN% appear to return to normal range. Thus, these findings demonstrate NiO NPs therapeutic effectiveness in a mouse model against *E. coli* and *S.aures.*

4. Conclusion

A facile and environment-affable approach was followed for the fabrication of highly crystalline NiO NPs, which exhibit high sur-

Table 1
Hematological analysis infected and treated mice models.

Parameters	*E. coli* infected mice	*E. coli*-NiO inoculated mice	*S. aureus* infected mice	*S. aureus*-NiO inoculated mice	Normal range
WBC	$13.7*10^9$/L	$2.2*10^9$/L	$8.8*10^9$/L	$5.7*10^9$/L	0.8–6.8
Lymph #	$4.2*10^9$/L	$1.6*10^9$/L	$4.7*10^9$/L	$3.8*10^9$/L	0.7–5.7
Mon#	$1.2*10^9$/L	$0.1*10^9$/L	$0.6*10^9$/L	$0.5*10^9$/L	0.0–0.3
Gran#	$8.4*10^9$/L	$0.5*10^9$/L	$3.5*10^9$/L	$1.4*10^9$/L	0.1–1.8
Lymph %	30.0 %	73.5 %	53.0 %	63 %	55.8–90.6
Mon%	8.8 %	3.9 %	7.7 %	5.2 %	1.8–6.0
Gran%	61.1 %	22.1 %	39.7 %	36.2 %	6.36–9.42
RBC	$9.24*10^{12}$/L	$19.66*10^{12}$/L	$8.45*10^{12}$/L	$18.46*10^{12}$/L	11.0–14.3
HGB	11.1 g/dl	12.1 g/dl	13.2 g/dl	13.2 g/dl	8.6–38.9
HCT	39.6 %	37.3 %	44.9 %	43.6 %	34.6–44.0
MCV	42.9fL(L)	53.9fL(L)	53.0fL	53.4fL(L)	48.2–58.3
MCH	12.0 pg(L)	16.1 pg(L)	15.5 pg(L)	17.2 pg(L)	15.8–19.0
MCHC	28.0 g/dL(L)	29.2 g/dL(L)	29.3 g/dL (L)	31 g/dL(L)	30.2–35.3
RDW	20.3 %(H)	19.3 %(H)	21.1 %(H)	19.5 %(H)	13.0–17.0
PLT	$2599*10^9$/L(H)	$656*10^9$/L(H)	$1016*10^9$/L(H)	$1016*10^9$/L(H)	450–1690
MPV	4.9fL	5.3 fL	5.5 fL	4.9 fL	3.8–6.0
PDW	15.7	15.9	16.6	15.1	–
PCT	–	0.150	0558 %	0.613 %	–

face area and a narrow band gap. The MICs of NiO NPs for of *S. aureus* (3.51 μg/mL) and *E. coli* (7.02 μg/mL) had provide a strong base for *in-vivo* and *in-vitro* antibacterial experiment. The in-vitro activity procured to increase with increasing NiO NPs concentration, which might be due to the maximum accumulation on the surface and penetration on the inside the cell. The 3×10^7 CUFs are tolerated concentration of both bacterial species that cause maximum infection (no death) in mice, whereas the 11 ppm suspension of NiO NPs had caused no damage to the mice. The concentration above 3×10^7 CUFs and 11 ppm was proved lethal and lead to the death of mice eventually. The results also reveal that after the inoculation of tolerated NiO dose, reduced the intensity of infection mice, which prove the antibacterial potency of NiO NPs.

Declaration of Competing Interest

The authors declare that they have no known competing financial interests or personal relationships that could have appeared to influence the work reported in this paper.

Acknowledgements

The authors extend their appreciation to the deanship of scientific research for funding this article by Taif University Research Supporting Project number (TURSP-2020/64), Taif University, Taif, Saudi Arabia.

References

Ahmadmoradi, E., Rezaie, A., Mousavi, S.M., 2012. Histopathological study of the kidney, liver and intestine tissues in goldfish (Carassius auratus) and angelfish (Pterophyllum sp.). AACL Bioflux 5, 282–288.

Akah, P., Alemji, J., 2009. Studies on the effects of Vernonia amygdalina leaf extract and fractions on biochemical and hematological parameters in diabetic rats. PlantaMedica 75. https://doi.org/10.1055/s-0029-1234707.

Al-Qayim, A.J.M., Ghali, L., Al-Azwai, T., 2014. Comparative effects of propolis and malic acid on hematological parameters of aluminum exposed male rats. Glob J Biosci Biotechnol 3, 6–11.

Anand, G.T., Nithiyavathi, R., Ramesh, R., John Sundaram, S., Kaviyarasu, K., 2020. Structural and optical properties of nickel oxide nanoparticles: Investigation of antimicrobial applications. Surf. Interfaces 18,. https://doi.org/10.1016/j.surfin.2020.100460 100460.

Angel Ezhilarasi, A., Judith Vijaya, J., Kaviyarasu, K., John Kennedy, L., Ramalingam, R.J., Al-Lohedan, H.A., 2018. Green synthesis of NiO nanoparticles using Aegle marmelos leaf extract for the evaluation of in-vitro cytotoxicity, antibacterial and photocatalytic properties. J. Photochem. Photobiol. B Biol. 180, 39–50. https://doi.org/10.1016/j.jphotobiol.2018.01.023.

Arora, B., Murar, M., Dhumale, V., 2015. Antimicrobial potential of TiO2 nanoparticles against MDR Pseudomonas aeruginosa. J. Exp. Nanosci. 10, 819–827. https://doi.org/10.1080/17458080.2014.902544.

Chen, J., Li, C., Guan, Y., Kong, Q., Li, C., Guo, X., Chen, Q., Jing, X., Lv, Z., An, Y., 2007. Protection of mice from lethal Escherichia coli infection by chimeric human bactericidal/permeability-increasing protein and immunoglobulin G1 Fc gene delivery. Antimicrob. Agents Chemother. 51, 724–731. https://doi.org/10.1128/AAC.00360-06.

Ezhilarasi, A.A., Vijaya, J.J., Kaviyarasu, K., Zhang, X., Kennedy, L.J., 2020. Green synthesis of nickel oxide nanoparticles using Solanum trilobatum extract for cytotoxicity, antibacterial and photocatalytic studies. Surf. Interfaces 20,. https://doi.org/10.1016/j.surfin.2020.100553 100553.

Gad, S.B., Zaghloul, D.M., 2013. Beneficial effects of green tea extract on liver and kidney functions, ultrastructure, lipid profile and hematological parameters in aged male rats. Global Veterinaria 11, 191–205. https://doi.org/10.5829/idosi.gv.2013.11.2.7472.

Gao, L., Yang, S.T., Li, S., Meng, Y., Wang, H., Lei, H., 2013. Acute toxicity of zinc oxide nanoparticles to the rat olfactory system after intranasal instillation. J. Appl. Toxicol. 33, 1079–1088. https://doi.org/10.1002/jat.2842.

Hafeez, M., Zeb, M., Khan, A., Akram, B., Abdin, Z.-u., Haq, S., Zaheer, M., Ali, S., 2021. Populus ciliata mediated synthesis of silver nanoparticles and their antibacterial activity. Microsc. Res. Tech. 84 (3), 480–488.

Haq, S., Rehman, W., Waseem, M., Javed, R., Mahfooz-ur-Rehman, Shahid, M., 2018. Effect of heating on the structural and optical properties of TiO2 nanoparticles: antibacterial activity. Appl. Nanosci. 8 (1-2), 11–18.

Haq, S., Ahmad, P., Khandaker, M.U., Faruque, M.R.I., Rehman, W., Waseem, M., Din, S.U., 2021a. Antibacterial, antioxidant and physicochemical investigations of tin dioxide nanoparticles synthesized via microemulsion method. Mater. Res. Express 8 (3), 035013.

Haq, S., Dildar, S., Ali, M.B., Mezni, A., Hedfi, A., Shahzad, M.I., Shahzad, N., Shah, A., 2021b. Antimicrobial and antioxidant properties of biosynthesized of NiO nanoparticles using Raphanus sativus (R. sativus) extract. Mater. Res. Express 8 (5), 055006.

Hein, M.S., 2003. Copper deficiency anemia and nephrosis in zinc-toxicity: a case report. S. D. J. Med. 54, 143–147.

Hunter, P.A., Rolinson, G.N., Witting, D.A., 1973. Comparative activity of amoxycillin and ampicillin in an experimental bacterial infection in mice. Antimicrob. Agents Chemother. 4, 285–293. https://doi.org/10.1128/AAC.4.3.285.

Iqbal, J., Abbasi, B.A., Mahmood, T., Hameed, S., Munir, A., Kanwal, S., 2019. Green synthesis and characterizations of Nickel oxide nanoparticles using leaf extract of Rhamnus virgata and their potential biological applications. Appl Organometal Chem 33 (8).

Isa khan, M., Nawaz, M., Bilal Tahir, M., Iqbal, T., Pervaiz, M., Rafique, M., Aziz, F., Younas, U., Alrobei, H., 2020. Synthesis, characterization and antibacterial activity of NiO NPs against pathogen. Inorg. Chem. Commun. 122, 108300.

Jasper, R., Locatelli, G.O., Pilati, C., Locatelli, C., 2012. Evaluation of biochemical, hematological and oxidative parameters in mice exposed to the herbicide glyphosate-roundup®. Interdiscip. Toxicol. 5, 133–140. https://doi.org/10.2478/v10102-012-0022-5.

Jeng, H.A., Swanson, J., 2006. Toxicity of Metal Oxide Nanoparticles in Mammalian Cells. J. Environ. Sci. Health A 41, 2699–2711. https://doi.org/10.1080/10934520600966177.

Kelly Nitsche, E., 2004. Erythrocytosis in Dogs and Cats: Diagnosis and Management. Compend. Contin. Educ. Pract. Vet. 26, 104–118.

Lingaraju, K., Raja Naika, H., Nagabhushana, H., Jayanna, K., Devaraja, S., Nagaraju, G., 2020. Biosynthesis of Nickel oxide Nanoparticles from Euphorbia heterophylla (L.) and their biological application. Arab. J. Chem. 13, 4712–4719. https://doi.org/10.1016/j.arabjc.2019.11.003.

Llobet, J.M., Domingo, J.L., Colomina, M.T., Mayayo, E., Corbella, J., 1988. Subchronic oral toxicity of zinc in rats. Bulletin of Environmental Contamination and Toxicology 41, 36–43. https://doi.org/10.1007/BF01689056.

Maruthupandy, M., Rajivgandhi, G.N., Quero, F., Li, W.-J., 2020. Anti-quorum sensing and anti-biofilm activity of nickel oxide nanoparticles against Pseudomonas aeruginosa. J. Environ. Chem. Eng. 8 (6), 104533.

Mayedwa, N., Mongwaketsi, N., Khamlich, S., Kaviyarasu, K., Matinise, N., Maaza, M., 2017. PT SC. Appl. Surf. Sci. https://doi.org/10.1016/j.apsusc.2017.12.116.

Mushtaq, S., Khan, J.A., Rabbani, F., Latif, U., Arfan, M., Yameen, M.A., 2017. Biocompatible biodegradable polymeric antibacterial nanoparticles for enhancing the effects of a third-generation cephalosporin against resistant bacteria. J. Med. Microbiol. 66, 318–327. https://doi.org/10.1099/jmm.0.000445.

Ramalingam, R., Hussain, M., Turabe, U., Kumar, N., Deivi, K., 2019. Green synthesis, characterization and antibacterial evaluation of electrospun nickel oxide nanofibers. Mater. Lett. 256,. https://doi.org/10.1016/j.matlet.2019.126616 126616.

Rehman, F.U., Mahmood, R., Ali, M.B., Hedfi, A., Almalki, M., Mezni, A., Rehman, W., Haq, S., Afsar, H., 2021. Bergenia ciliate–Mediated Mixed-Phase Synthesis and Characterization of Silver-Copper Oxide Nanocomposite for Environmental and Biological Applications. Materials 14 (20), 6085.

Rodrigues, J.M., Fessi, H., Bories, C., Puisieux, F., Devissaguet, J. ph, 1995. Primaquine-loaded poly(lactide) nanoparticles: physicochemical study and acute tolerance in mice. International Journal of Pharmaceutics 126, 253–260. https://doi.org/10.1016/0378-5173(95)04135-4.

Saravanan, M., Selvaraj, A., Lakshmi, T., Arivalagan, P., 2018. Synthesis of silver nanoparticles from Phenerochaete chrysosporium (MTCC-787) and their antibacterial activity against human pathogenic bacteria. Microb. Pathog. 117, 68–72. https://doi.org/10.1016/j.micpath.2018.02.008.

Shah, A., Haq, S., Rehman, W., Muhammad, W., Shoukat, S., Rehman, M. ur, 2019. Photocatalytic and antibacterial activities of Paeonia emodi mediated silver oxide nanoparticles. Materials Research Express 6, 045045. doi:10.1088@2053-1591@aafd42.

Shanker, K., Mohan, G.K., Hussain, M.A.M., Jayarambabu, N., Pravallika, P.L., 2017. Green Biosynthesis, Characterization, In vitro Antidiabetic Activity, and Investigational Acute Toxicity Studies of Some Herbal-mediated Silver Nanoparticles on Animal Models. Phcog Mag 13, 188–192. https://doi.org/10.4103/0973-1296.197642.

Teeguarden, J.G., Hinderliter, P.M., Orr, G., Thrall, B.D., Pounds, J.G., 2007. Particokinetics in vitro: Dosimetry considerations for in vitro nanoparticle toxicity assessments. Toxicological Sciences. doi:10.1093/toxsci/kfl165.

Wang, D., Li, H., Liu, Z., Zhou, J., Zhang, T., 2017. Acute toxicological effects of zinc oxide nanoparticles in mice after intratracheal instillation. Int. J. Occup. Environ. Health 23, 11–19. https://doi.org/10.1080/10773525.2016.1278510.

Zarei, Z., Razmjoue, D., Karimi, J., 2020. Green Synthesis of Silver Nanoparticles from Caralluma tuberculata Extract and its Antibacterial Activity. J. Inorg. Organomet. Polym Mater. 30 (11), 4606–4614.